Medullary astrocytes mediate irregular breathing patterns generation in chronic heart failure through purinergic P2X7 receptor signalling

Camilo Toledo,[a,d] Esteban Díaz-Jara,[a] Hugo S. Diaz,[a] Karla G. Schwarz,[a] Katherin V. Pereyra,[a] Alexandra Las Heras,[a] Angélica Rios-Gallardo,[a] David C. Andrade,[a,b] Thiago Moreira,[e] Ana Takakura,[f] Noah J. Marcus,[g] and Rodrigo Del Rio [a,c,d]*

[a]Laboratory of Cardiorespiratory Control, Department of Physiology, Pontificia Universidad Católica de Chile, Alameda 340, Santiago, Chile
[b]Centro de Fisiología y Medicina de Altura, Facultad de Ciencias de la Salud, Universidad de Antofagasta, Antofagasta, Chile
[c]Centro de Envejecimiento y Regeneración (CARE), Pontificia Universidad Católica de Chile, Santiago, Chile
[d]Centro de Excelencia en Biomedicina de Magallanes (CEBIMA), Universidad de Magallanes, Punta Arenas, Chile
[e]Department of Physiology and Biophysics, Institute of Biomedical Science, University of Sao Paulo, Sao Paulo, SP, Brazil
[f]Department of Pharmacology, Institute of Biomedical Science, University of Sao Paulo, Sao Paulo, SP, Brazil
[g]Department of Physiology and Pharmacology, Des Moines University, Des Moines, IA, USA

Summary

Background Breathing disorders (BD) (apnoeas/hypopneas, periodic breathing) are highly prevalent in chronic heart failure (CHF) and are associated with altered central respiratory control. Ample evidence identifies the retrotrapezoid nucleus (RTN) as an important chemosensitivity region for ventilatory control and generation of BD in CHF, however little is known about the cellular mechanisms underlying the RTN/BD relationship. Within the RTN, astrocyte—mediated purinergic signalling modulates respiration, but the potential contribution of RTN astrocytes to BD in CHF has not been explored.

Methods Selective neuron and/or astrocyte-targeted interventions using either optogenetic and chemogenetic manipulations in the RTN of CHF rats were used to unveil the contribution of the RTN on the development/maintenance of BD, the role played by astrocytes in BD and the molecular mechanism underpinning these alterations.

Findings We showed that episodic photo-stimulation of RTN neurons triggered BD in healthy rats, and that RTN neurons ablation in CHF animals eliminates BD. Also, we found a reduction in astrocytes activity and ATP bioavailability within the RTN of CHF rats, and that chemogenetic restoration of normal RTN astrocyte activity and ATP levels improved breathing regularity in CHF. Importantly, P"X/ $P2X_7$ receptor ($P2X_7r$) expression was reduced in RTN astrocytes from CHF rats and viral vector-mediated delivery of human P2X7 $P2X_7r$ into astrocytes increases ATP bioavailability and abolished BD.

Interpretation Our results support that RTN astrocytes play a pivotal role on BD generation and maintenance in the setting CHF by a mechanism encompassing $P2X_7r$ signalling.

*Corresponding author at: Laboratory of Cardiorespiratory Control, Department of Physiology, Pontificia Universidad Católica de Chile, Alameda 340, Santiago, Chile.
E-mail address: rdelrio@bio.puc.cl (R. Del Rio).

Introduction

Chronic Heart failure (CHF) is associated with a high incidence of abnormal breathing patterns (i.e., Cheyne-stokes respiration) which are closely related to poor prognosis and higher mortality.[1] Previous studies suggest that the pathophysiology of abnormal breathing patterns in CHF is linked in part to abnormal central

Research in context

Evidence before this study

Disordered breathing (i.e. apnoeas/hypopneas, periodic breathing) are highly prevalent in chronic heart failure (CHF), one of the most prevalent cardiovascular diseases among the elderly population worldwide. Despite, the precise mechanisms underlying breathing disorders generation in the setting of cardiac failure are still not known; however, alterations in ventilatory chemoreflex drive has been closely linked to unstable breathing in CHF and disease progression. Recent evidence showed the contribution of astrocytes (residing within brainstem chemoreceptor areas) on breathing regulation and its dependence on ATP signalling. Indeed, purinergic signaling in the retrotrapezoid nucleus (RTN), a main brainstem region for ventilatory chemoreflex regulation, can modulate chemoreceptor neurons activity and breathing. Yet, nothing is known about the role of astrocytes and/or purinergic signalling on disordered breathing during CHF progression.

Added value of this study

This is the first study assessing the contribution of medullary astrocytes on the development/maintenance of disordered breathing in non-ischemic CHF. Here we showed that experimental CHF rats displayed metabolic inhibition of RTN astrocytes and decreased ATP-related signalling at the RTN triggering irregular breathing. Accordingly, restoration of normal astrocyte activity using chronic chemogenetic activation normalized breathing in CHF. Altered purinergic signalling in the RTN of CHF rats was linked to downregulation of astrocytic P2X7r and P2X7r^{-}/$^{-}$ knockout mice mimics the respiratory phenotype observed in CHF. Finally, transgene delivery of the human P2X7r selectively into RTN astrocytes increases ATP bioavailability and completely abolished disordered breathing in CHF.

Implications of all the available evidence

Our results strongly support the role of RTN astrocytes in the maintenance of disordered breathing in CHF by a mechanism encompassing purinergic signaling through the P2X7r. Our work represents an advance in the understanding of the generation of breathing disorders during CHF progression and provides comprehensive and mechanistic insights for the future development of novel strategies to reduce breathing disorders in the setting of CHF.

chemoreflex function and attendant instability in the respiratory control system.[2−4] Central chemoreceptors, which play an important role in respiratory control, respond to subtle changes in brain PCO_2 to minimize acid-base changes and provide a tonic drive to breathe under eupneic conditions.[5−7] The molecular identity of the sensors that mediate central respiratory chemoreception has been extensively studied in the retrotrapezoid nucleus (RTN) since it is considered a major nodal point for regulation of respiration during variations in brain PCO_2.[8,9] Indeed, the 2-pore domain K$^+$ background channel TASK-2 and the G-coupled proton sensor GPR4 has both been implicated in H$^+$ sensing in RTN chemoreceptor neurons.[10] Despite the intrinsic chemo-sensitive properties of RTN neurons, recent evidence supports the role of glial cells on the regulation of breathing.[11−13] Particularly, the role of RTN astrocytes has received great attention in the recent years in the field of central chemoreception.[14,15]

Astrocyte-derived ATP acting on purinergic receptors has been proposed to play an important role in respiratory regulation, and there is increasing evidence indicating astrocytes as the main source for purinergic drive at the RTN level.[16] It has been shown that astrocytes residing in the RTN respond to physiological decreases in pH with vigorous elevations in intracellular Ca^{2+} and release of ATP which in turn activates RTN neurons inducing adaptive increases in breathing.[11] Furthermore, applications of selective purinergic P2X receptor blockers into the RTN reduced respiratory response to increasing CO_2 levels but also causes irregular breathing patterns at rest,[17] suggesting that purinergic signalling within the RTN contributes to eupnoeic respiratory rhythm. This notion has not been rigorously tested in physiological or pathological settings. Accordingly, the potential role of astrocytes in modulating RTN function in the setting of CHF, as well as the molecular mechanisms involved in this process have not been explored. Recently, we showed that ablation of RTN neurons in experimental CHF completely restores normal central chemoreflex function.[18] Importantly, the existence of an RTN-like structure has been documented in humans, increasing translational potential of basic research associated with RTN function.[19,20] Despite the fact that the role of the RTN in regulating the hypercapnic ventilatory response is well established, the mechanisms involved in RTN-mediated regulation of ventilation at rest in CHF remains largely unknown.

Therefore, the aims of the present study were to determine the contribution of the RTN and examine the role of astrocytes on disordered breathing in experimental CHF. Since it has been shown that astrocyte-derived ATP played a role in the regulation of altered neuronal function in myocardial infarcted rats,[21] we also aimed to determine whether astrocyte-mediated purinergic signalling contribute to the development/maintenance of breathing disorders in CHF. To address these aims we used a combination of several physiological and molecular approaches in a non-ischemic volume overload model of CHF. We chose this model because it recapitulates disordered breathing and chemoreflex alterations observed in human CHF without the potential confounding influence of decreases in brain perfusion.[22] In this study we reveal a novel molecular mechanism that

governs disordered breathing in experimental CHF. Our studies demonstrate that astrocytic P2X7 receptors (P2X7r) in the RTN play a pivotal role in generation of irregular breathing patterns observed in CHF rats. More importantly, we show that cell-targeted upregulation of astrocyte P2X7r in the RTN of CHF animals completely normalizes irregular breathing patterns.

Methods

Animals

Experiments were performed using adult male Sprague Dawley rats (n=80) obtained from colonies maintained at the animal facility of the Pontificia Universidad Católica de Chile. Analyses were carried out when the rats reached 16 weeks of age. Adult male P2X7r knock-out mice (n=13) generated by Gabel's group at Pfizer were obtained from Jackson Laboratory (IMSR_JAX:005576) to establish an in-house colony. C57BL/6J mice (RRID:IMSR_JAX:000664) were used as wild type (n=9). Analyses in mice were performed at 12 weeks of age. All animals/samples were simultaneously randomised to the treatment groups without considering any other variable. The animals were group-housed and maintained on a 12-h light cycle (lights on 07:00) and had ad libitum access to water and food. The animals were housed in a temperature-controlled room at $23\pm1°C$ with $60 \pm 5\%$ relative humidity. The number of animals per experimental group were calculated to obtain a statistical power between 0.9 to 1.0 $(1-\beta)$, which rules out false positives in our results, and determined in relation to statistical difference observed in our previous studies.

Animal preparation for the *in vivo* studies

Brain injections and fibre optic implantation were performed on a stereotaxic frame (David Kopf Instruments, model 940). Animals were anesthetized with an intraperitoneal injection of a mixture 3:1 of ketamine (100 mg/kg) and xylazine (10 mg/kg), respectively. For chronic heart failure induction, echocardiography, mini-osmotic pump (Alzet, 2ML2 model) implantation, and telemetry transmitter (Data Science International, HD-S10 model) implantation, rats were anesthetized with isoflurane (5% for induction, 2% for maintenance, balanced with O_2). During surgery, animals were maintained at $36\pm1°C$ using a homeothermic monitoring system (ThermoStar, RWD). In all animals, incisions were closed in two layers using absorbable sutures for internal closures (BBraun, Vycril 4-0), and steel clips for skin. Antibiotic (enrofloxacine, 100 mg/kg, s.c) and analgesic (ketoprofen, 5 mg/kg, s.c.) were administered every 24 h for 3 days following surgery. At the end of experimental protocol, all animals were humanely euthanized with an overdose of sodium pentobarbital (100 mg/kg, i.p.).

Heart failure model

Non-ischemic heart failure was induced by the surgical creation of an arteriovenous (A-V) fistula as previously described.[22–25] Briefly, rats were anesthetized (isoflurane 2%, balanced with O_2) and the inferior vena cava and the abdominal aorta were exposed using a midline incision. Both vessels were clamped, caudal to the renal artery and to the aortic bifurcation, respectively. The aorta was punctured using an 18-gauge needle and advanced until it perforated the adjacent vena cava. Immediately afterward, a drop of Histoacryl glue (BBraun, cat# 1050052) was used to seal the aorta at the puncture point. In the control group, the sham surgery was done in the same manner as described above except there was no creation of an A-V fistula. No significant changes in arterial blood gases have been previously reported in A-V fistula rats.[18,23]

Echocardiography

Longitudinal evaluation of cardiac function during the progression of CHF (4 and 8-weeks post CHF induction) was performed in anesthetized rats (isoflurane 2%, balanced with O_2) using transthoracic M-mode echocardiography at the level of the mid-papillary muscle using a parasternal short-axis view (Mindray Z6 Vet). The criterion for establishment of the CHF model was an increase in left ventricle end-diastolic volume (EDV) and stroke volume (SV) (>2-fold) relative to Sham without changes in ejection fraction (EF).[25,26] Prior to treatments performed at 4 weeks, rats that met the criteria (85% of total fistulated animals) for CHF were selectively grouped to sure ensure equal grade of cardiac dysfunction.

Lesions with substance P-conjugated saporin

At 4-weeks post-CHF or Sham surgery, rats were anesthetized (ketamine 100 mg/kg; and xylazine 10 mg/kg, i.p.) and fixed to a stereotaxic frame. Bilateral injections of saporin toxin conjugated to substance P (SSP-SAP; 0.6 ng/30 nl; Advanced Targeting Systems, cat# IT-11) were administered into the RTN to destroy neurons that express substance P receptors (NK1R). SSP-SAP dose was selected based on previous studies showing a 60-70% ablation of pH-sensitive neurons that expresses the transcription factor Phox2b and are non-catecholaminergic (Phox2b+TH−) in the RTN of rats.[18,27] Facial motoneurons, catecholaminergic and serotonergic neurons, and neurons located in the ventral respiratory column caudal to the facial motor nucleus are not affected by these injections. Three separate injections of SSP-SAP were placed 2.0 mm lateral, 2.4±0.2 mm caudal to lambda and 8.5 mm ventral from the surface of the

brain, as previously reported,[28] and according to *The Rat Brain in Stereotaxic Coordinate*,[29] using a Hamilton syringe (0.5 μL, Neuros Syringe, Model 7000.5 KH, 32 gauge, Point Style 3, part# 65457-01) connected to controlled flow injection (2 nl/seg, Microinjection Syringe Pump, part# UMP3T-2, WPI). Vehicle operated rats were injected with sterile saline solution. No significant changes in arterial blood gases have been previously reported in A-V fistula rats after SSP-SAP administration.[18]

Injection of lentivirus and instrumentation

A lentiviral vector (LVV) carrying the Phox2b-responsive promoter PRSX8 and an enhanced version of the photo-activable cationic channel channelrhodopsin2 (ChR2 H132R) fused to eYFP (pLenti-PRSX8-ChR2(H132R)-eYFP; Construct: Ruth Stornetta, University of Virginia, Addgene plasmid cat# 89539) was used for photoactivation of RTN neurons.[30] LVV was produced at 1.2×10^9 viral particles/ml kindly provided by Dr. Thiago Moreira, University of Sao Paulo. A volume of 450 nl (150 nl in 3 sites separated by 200 μm along the anterior−posterior axis) containing LVV-PRSX8-ChR2 (H132R)-eYFP was injected unilaterally into RTN (2.0 mm lateral, 2.4±0.2 mm caudal to lambda and 8.5 mm ventral from the surface of the brain) of four healthy rats (300 ± 10 g) by controlled flow injection (2 nl/seg) using a Hamilton syringe (0.5 μl) connected to an injection needle (32 gauge). As a control, an LVV not carrying ChR2(H132R) was injected in the contralateral side (Vehicle; 150 nl in 3 sites separated by 200 μm along the anterior−posterior axis). This vector was used solely to control for possible nonselective effects of photo- stimulation in this region of the brain. After virus injection, two optical fibres (Cannula 2.5 mm; Silica 200 μm; NA 0.66; Protrusion length 8.5mm; Prizmatix Ltd) assemblies were implanted into the RTN (tips 0.3 mm dorsal to the vector injection site) and fixed to the cranium using dental cement and jeweler's screws as previously described.[31] Animals were maintained for no less than 4 weeks before they were used in physiological experiments. The surgical procedures and virus injections produced no observable behavioural or respiratory effects and these rats gained weight normally.

Designer receptors exclusively activated by designer drugs (DREADDs)

Ready-to-use adeno-associated virus serotype 5 (AAV5) particles (titter: 7×10^{12} vg/ml) produced from pAAV-GFAP-hM3D(Gq)-mCherry (Construct: Bryan Roth, UNC Chapel Hill, Addgene plasmid cat# 50478) was used to chronically activate astrocytes.[32] Briefly, 450 nl of solution (150 nl in 3 sites separated by 200 μm along the anterior−posterior axis) containing AAV5-GFAP-

hM3D(Gq)-mCherry was delivered bilaterally into the RTN (1.8 mm lateral, 2.4±0.2 mm caudal to lambda and 8.5 mm ventral from the surface of the brain) at 4 weeks post-CHF induction in six rats (350 ± 20 g) by controlled flow injection (2 nl/seg, Syringe infusion pump, KD scientific) using a Hamilton syringe (0.5 μl) connected to an injection needle (32 gauge). After 2 weeks of virus injections, a mini-osmotic infusion pump (Alzet, 2ML2 model) loaded with 2 mL clozapine N-oxide dihydrochloride (CNO, 100mM; HelloBio Inc, cat# HB6149) was surgically implanted (s.c.) for constant CNO administration (5μL/h for 14 days). Animals were maintained for 2 weeks before they were used in physiological experiments. As a control, an AAV not carrying DREADDS (AAV5-GFAP.eGFP.WPRE.hGH, Addgene cat#105549) was injected bilaterally in the RTN of six CHF control rats. This vector was used solely to control for possible nonselective effects of constitutive activity of overexpressed DREADD receptors and for DREADD-independent effects of CNO. To control for this last possibility, we confirmed that CNO infusion did not have effect on cardiorespiratory physiology.

P2X7r adeno-associated virus

Customized AAV serotype 5 constructs containing the P2X7 receptor gene (NM_019256.1) under the control of GFAP promoter fused to GFP (AAV5-GFAP-P2X7r-P2A-GFP, 1×10^{13} vg/ml) were packaged and purified by VIROVEK's AAV production system. A volume of 450 nl (150 nl in 3 sites separated by 200 μm along the anterior−posterior axis) containing AAV5-GFAP-P2X7r-P2A-GFP was delivered bilaterally into the RTN (1.8 mm lateral, 2.4±0.2 mm caudal to lambda and 8.5 mm ventral from the surface of the brain) at 4 weeks post-CHF induction in six rats (350 ± 20 g) by controlled flow injection (2 nl/seg) using a Hamilton syringe (0.5 μl) connected to an injection needle (32 gauge). Animals were maintained for 3 weeks before they were used in physiological experiments. As a control, 450 nl of AAV5-GFAP.eGFP.WPRE.hGH virus was injected bilaterally in six CHF+Ctrl rats. This vector was used solely to control for possible nonselective effects of viral transfection in this region of the brain. In P2X7r knockout mice three AVV injections (total volume: 300 nl) were delivery bilaterally into the RTN at 6.6± 0.15 mm caudal to bregma, 1.5 mm lateral to the midline, and 4.6 mm below the dura mater according to *The Mouse Brain Atlas in Stereotaxic Coordinate*,[33] using a Hamilton syringe (0.5 μl) connected to a 32-gauge injection needle with controlled flow injection (2nl/seg).

Ventilatory chemoreflex function

All the experiments were performed between 10:00 and 16:00 h, at an ambient room temperature of 24±2° C. Animals were habituated to a whole-body

plethysmography chamber (5 L, EMKA Technologies) for two consecutive days prior to recording. On the day of the experiment, a minimum of 2 h was allowed for the rat to acclimatize to being in the chamber prior to initiation of measurements. Respiratory flow was recorded with a differential pressure transducer. The signal was amplified (X500) and digitized at 1 kHz. Area of the curve of the inspiratory flow was calibrated by injecting 5 mL of dry air into the chamber with a syringe. Tidal volume (V_T), respiratory frequency (R_f), minute ventilation (V_E: V_T x R_f), inspiratory time (T_i), expiratory time (T_e), total respiratory time (T_{TOT}), respiratory drive (V_T/T_i), peak inspiratory flow (PiF) and peak expiratory flow (PeF) were analyzed by using ECGauto software (EMKA technologies, France) as previously described.[24,26] Central chemoreceptors were stimulated by exposures to hyperoxic hypercapnia (7% CO_2−93% O_2) gas challenges given for 10 min (2 min for mice). The input and output flow were 2.0 l/min and 1.5 l/min, respectively. The hypercapnic ventilatory response (HCVR) was obtained by calculating the slope of the V_E between F_iCO_2 0.03% and 7%. The ventilatory response-curves were fitted to the inspiratory CO_2 according to the following exponential function: $V_E = K*exp(F_iCO_2) + plateau$. All recordings were made at an ambient temperature of $25 \pm 2°C$. By convention, in all representative tracings, a negative deflection in the flow signal represents inspiration and a positive deflection in the flow signal represents expiration.

Breathing irregularity

Recordings were made between 10.00 and 16.00 h. Resting breathing was recorded over the course of 2h while the rats breathed room air in the plethysmograph chamber. All ventilatory variables were analysed during the last hour of the recording to make sure the animals were sleeping (periods of sleep evidenced by non-activity-related events assessed by radio-telemetry units combined with video monitoring). Breathing patterns were evaluated by an unbiased investigator related to group/condition/treatment animal allocation. Respiratory stability at rest was assessed by construction of Poincare plots and quantified by analysis of SD1 (standard deviation 1) and SD2 (standard deviation 2) of the breath-to-breath interval variability over six different random segments of 400 consecutive breaths. V_T oscillations were analysed by the calculation of the coefficient of variation of the magnitude of each V_T cycle in the same respiratory segments.[26] In addition, an index of breathing variability was calculated using the irregularity score (IS) as described previously.[34−36] Briefly, IS was calculated as a percentage using the following equation: $100 \times ABS (T_{TOTn} − T_{TOTn−1})/T_{TOTn−1}$ for the nth respiratory cycle. A lower irregularity score indicates a more regular respiratory rhythm. Breathing disorders were quantified during 1 h of resting breathing as previously described.[26]

Briefly, spontaneous apnoeas were defined as the cessation of breathing for at least three respiratory cycles, as determined by respiratory rate for the prior 10 s; hypopneas were defined as reductions in breath amplitude <50% of the normal V_T, for at least three respiratory cycles, as determined by V_T amplitude average of the preceding 10 s of regular breathing; sighs, were defined as a breath cycle with amplitude >50% of the average cycle amplitude of the preceding 10 s of regular breathing; post-sigh apnoea's were defined as the cessation of breathing for at least three respiratory cycles immediately after a sigh. Duration of apnoeas, hypopneas and post-sigh apnoea's was quantified as well.

Photo-stimulation

On the day of the recordings, rats were briefly anesthetized with isoflurane (5% balanced in O_2 for 3 min) to connect the head fibre optic leads to a fibre optic patch cord (Prizmatix Ltd) and then animals were placed in the ventilatory chambers for unrestrained whole-body plethysmography (5 L, EMKA Technologies). A minimum of 1 h was allowed for rats to recover after connecting the fibre optic patch cord to the power source. Photo-stimulation of ChR2-expressing RTN neurons was performed using an Ultra High-Power LED (460 nm) with UHP-Mic-LED Current Controller (Prizmatix Ltd). For optogenetic activation trains of pulses were controlled by pulse train generator software (Pulser 2.3.1, Prizmatix Ltd). Stimulation consisted of 10 ms pulse duration delivered at 20 Hz applied during episodes of 30 s as previously described [37]. Laser output measured at the tip of the fibre was set at 12 mW prior to the insertion of the fibre in each experiment. Stimulation trains were applied every 6 min over the course of 1 h. The power setting of the light was kept constants for all experiments.

Active expiration

The presence of active expiration was identified as previously described.[38] Briefly, six segments of resting breathing were randomly chosen by an investigator blinded to group assignment. From these segments 300 consecutive respiratory cycles were analysed. We evaluated the total volume of expired air during the respiratory cycle by analysing the area under the curve of respiratory flow. To determine the presence of forced breaths, the expiratory phase was divided into two parts: early expiration (E1), corresponding to the initial 50% of the total expiratory time; and late expiration (E2), corresponding to the final 50% of the total expiratory time. Increases in the ratio between E2 and E1 expiratory phases (E2/E1) was used as the indicator of active expiration. Analyses were performed using a custom routine written in MATLAB (The MathWorks, Inc.).

qPCR

Rat brains were immediately removed after endpoint physiological experiments, frozen in liquid nitrogen and stored at $-80°C$ for subsequent use. Frozen brainstem containing RTN neurons were obtained by cutting $600-\mu m$ of coronal section through the medulla oblongata between 11.9 to 11.3 mm caudal to bregma using a cryostat. The RTN was punched using a blunt 15−gauge needle attached to a syringe as previously described.[23,24] RNA isolation and cDNA synthesis were performed using the RNAqueous Micro® (cat# AM1931, Ambion) and iScript® (cat# 1725037 Promega) kits respectively, according to manufacturer instructions. RNA purity was assessed by spectrophotometry through the 260/280 ratio (1.88 ± 0.11). Gene expression was assessed by SYBR green chemistry real-time PCR following reverse transcription of total RNA. Real-time PCR was performed using the ABI prism 7700 Sequence Detection System (Applied Biosystems). β-Actin mRNA was quantified as an internal control for each sample and quantifications were performed using the 2-$\Delta\Delta$CT method.

Western blot

Brainstem was dissected on ice and immediately frozen at $-80°C$. Then, coronal sections were cut at the level of the RTN (11.6±0.3 mm caudal to bregma) using a Leica CM3050S cryostat. Samples (50μg) were resolved by 10 % SDS-PAGE (Bio-Rad) and transferred to a PVDF membrane (Immobilon-P, cat# IPVH00010 Millipore). Chronic neuronal activation was assessed with a rabbit mAb anti-FosB (1:1000 dilution; cat# 2251, Cell Signalling Technology). Astrocyte activation was assessed with a rabbit mAb anti-Glial Fibrillary Acidic Protein (GFAP) (1:2000 dilution; cat# Z0334, DAKO). Astrocyte density was assessed with a mouse mAb S-100β (1:1000 dilution; cat# sc-393919 Santa Cruz Biotechnology). P2X7r expression was assessed with a rabbit mAb anti-P2X7r (1:1000 dilution, cat# KP11801, Calbiochem). Following stripping procedure (Restore Plus, cat# 46430, Thermo Scientific), the membranes were probed with a mouse mAb anti-β-actin antibody (1:2000; Sigma). Next, membranes were incubated 1h to room temperature with horseradish peroxidase-conjugated goat secondary antibody as appropriate (anti-rabbit, cat# 074−1506, KPL; anti-mouse, cat# 074-1806, KPL) for 1 h at room temperature. A C-DiGit Blot Scanner (LI-COR) was used as detection system, and the images were analysed with the software image studio lite version 5.2. The relative amount of protein of interest was calculated as the ratio of intensity of the band relative to the intensity of β-actin.

ATP determinations

ATP levels in the RTN were determined by a quantitative bioluminescence assay (cat# A22066, Invitrogen) according to manufacturer's instructions. Briefly, tissue was lysed with RIPA buffer containing ATPase inhibitor on ice for 10 min.[39] Reaction solution containing 1X reaction buffer, 1 mM DTT, 0.5 mM D-luciferin, 1.25 μg/ml firefly luciferase was prepared. 10 μL of supernatant was mixed with 100 μL reaction solution in white 96 well plate and then measured for luminescence at 560 nm using Synergy HTX microplate reader (Bio-Tek). Blank reaction and standard ATP solution was included as controls.

Immunofluorescence

Animals were deeply anaesthetized with urethane (40 mg kg−1 i.p.) and perfused through the ascending aorta with saline solution (NaCl 0.9%) followed by 4% phosphate-buffered (0.1 M; pH 7.4) paraformaldehyde (cat# P6148, Merck). The brain was removed and stored in the perfusion fixative for 3 h at room temperature and later maintained in 30% sucrose prior to cryopreservation. All histochemical procedures were performed using free-floating sections (30μm). To identify P2X7r and NMB mRNA, we used multiplex ISH with RNA-scope (probe cat# 458841 and 494791, respectively; Advanced Cell Diagnostics) according to the manufacturer's directions. Sections were briefly washed in sterile PBS 1X, mounted on charged slides, and dried overnight.[40] For fluorescence immunohistochemistry, sections were rinsed, then incubated in a Tris-buffered solution of 1% Bovine Serum Albumin, 0.5% Triton-X, and 150 mM sodium chloride, and then rinsed and incubated with primary antibody at 4°C overnight. GFAP were detected with a rabbit mAb GFAP (1:1000 dilutions, cat# Z0334, DAKO). TH and Phox2b were detected with mouse and rabbit antibodies, respectively (TH: 1:2000 dilution; Chemicon; Phox2b: 1:800 dilution; gift from J.F. Brunet, EcoleNormale Superieure, France). Sections were then rinsed and incubated with secondary antibody (goat anti-mouse Alexa 488, Invitrogen; donkey anti-rabbit Alexa 594, Jackson ImmunoResearch Laboratories) for 60 min and rinsed again before mounting on slides. ChR2-eYFP was detected by enhanced green fluorescent protein (eGFP) immunoreactivity, using mouse anti-GFP antibody (1:2000, cat# 11814460001 Roche), followed by goat anti-mouse Alexa 488 (1:500; Invitrogen) as previously described.[41] Slides were covered with ProLong Gold with DAPI anti-fade mounting medium (cat# P36931, Thermo Scientific).

Cell counting and imaging

A Zeiss 710 microscope was used to image the sections and perform subsequent analysis. Immunofluorescence was examined under epifluorescence illumination. The locations of TH and Phox2b marked in the retrotrapezoid nucleus region were plotted in sections from 10.40 to 12.08 mm caudal to bregma (8 sections/animal). The

profile counts of the animals that received bilateral microinjections of SSP-SAP were compared with the vehicle rats. The ZEN Image Analysis module was used for cell counting. QuPath, quantitative open-source software was used to estimated RNA probe expression according to manufacturing instruction.

Statistics
The statistical analysis was performed with GraphPad Prism 8.0 statistical software. Figures were designed using the vector graphics editor CorelDRAW X7. Normal distribution of the data was assessed with the Shapiro-Wilk normality test. Statistical significance of data with normal distribution was evaluated using unpaired Student's t test or one-way ANOVA test, followed by a Sidak post-hoc analysis, as mentioned in text. Correlations were performed using Pearson analysis. All P values are reported either in the text or in corresponding figure legends. Data are presented as mean ± standard error (SE) in text and tables. A P value of ≤ 0.05 was considered statistically significant.

Ethics approval
All experiments were performed in accordance with the Guide for the Care and Use of Laboratory Animals published by the US National Institutes of Health (NIH Publication eighth edition, update 2011). All experimental protocols were approved by the IACUC from the Pontificia Universidad Católica de Chile (protocol ID #170710022). All efforts were made to reduce the number of animals used and to minimize animal suffering.

Role of the funding source
The funders had no role in the study design, data collection, data analysis, interpretation of results, or writing of the report.

Results

Role of RTN in pathophysiology of breathing disorders in heart failure
Increased chemosensitivity to hypercapnia associated with breathing instability is considered a serious adverse prognostic factor in CHF patients.[2−4] Accordingly, we used experimental CHF rats to assess the contribution of RTN neurons to breathing disorders.[18,23,26,42] CHF rats showed overt signs of cardiac hypertrophy compared to control rats (Supplementary Table 1). As previously reported, CHF rats display: (i) enhanced ventilatory response to hypercapnia (HCVR), a measure of central chemoreflex sensitivity (Figures 1A, B; S1b,c), (ii) respiratory rhythm irregularity (Figure 2a−c), (iii) oscillatory breathing patterns characterized by fluctuations in tidal volume (V_T)

amplitude (Figure 2a,c,e), and iv) a higher apnoea/hypopnea index (AHI) (Figure 2a,f). Importantly, the enhanced HCVR was positively correlated with AHI in CHF rats but not in control rats (Figure S1d). Then, to test whether RTN neurons are necessary for central chemoreflex potentiation (i.e., enhanced HCVR) and disordered breathing in the setting of CHF, we selectively ablated RTN neurons using substance P-conjugated saporin toxin (SSP-SAP) (Figure S1a). Partial lesions of RTN neurons completely normalized the enhanced HCVR in CHF rats (Figure 1a−c). Notably, elimination of RTN neurons in CHF rats resulted in marked improvements in breathing regularity (Figure 2a−e) and significant decreases in AHI to levels comparable to those obtained in control rats (Figure 2f; Supplementary Table 2). In addition, the respiratory late: early expiration phase ratio, an index of forced breathing, was increased in CHF and this was dependent on the integrity of RTN neurons since partial ablation of RTN neurons in CHF rats abolished forced breathing (Figure 1d, e). Approximately 60% of RTN chemoreceptor neurons ($Phox2b^+/TH^-$) were destroyed by SSP-SAP toxin treatment (Figure 1f,g). No changes in baseline ventilatory parameters nor in upper airway permeability index were found between groups (Supplementary Table 3). Together, these results support a previously undocumented role for RTN chemoreceptor neurons contributing to the generation of disordered breathing in CHF.

Episodic photo-stimulation of RTN chemoreceptor neurons induces irregular breathing
During periodic breathing in CHF the alternating pattern of apnoeas can induce repetitive activation of chemoreceptors due to oscillations in P_aCO_2 creating a putative positive feedback loop that perpetuates breathing irregularities.[43,44] The contribution of RTN chemoreceptor neurons to this phenomenon has not been thoroughly tested. To evaluate the impact of repetitive stimulation of RTN neurons on breathing regularity, we selectively expressed the light-sensitive cation channel channelrhodopsin-2 into RTN chemoreceptor neurons (Figure S2). Consistent with previous observations,[31,37,45] high frequency photo-stimulation of RTN neurons produced acute increases in ventilation (Figure 3a,f). Notably, after RTN photo-stimulation breathing pattern became progressively more irregular compared to the pre-stimulation condition. This irregularity was characterized by increases in breath-to-breath interval variability and fluctuations in the amplitude of each ventilatory cycle (i.e., non-symmetrical distribution of the V_T histogram) (Figure 3d,i). As shown previously,[18,46] repetitive stimulation of RTN neurons induced a progressive decline in baseline ventilation, but these decreases in ventilation were accompanied by a progressive increase in irregularity scores (IS) (Figure 3j,l). Importantly, it has been proposed that
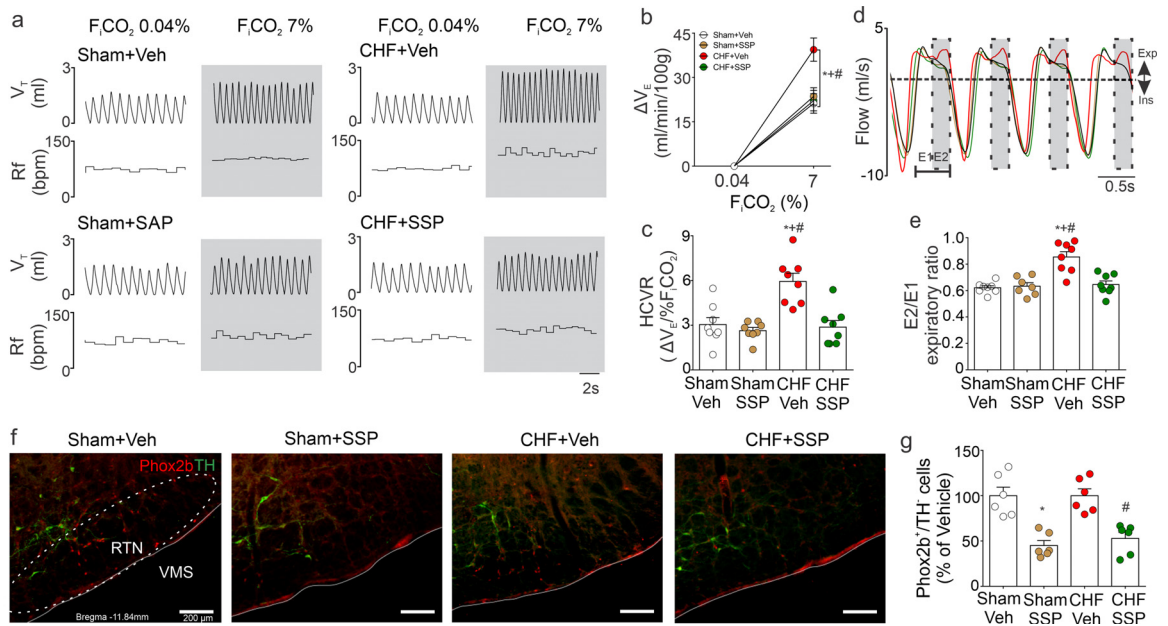
Figure 1. RTN neurones are required for the enhanced central chemoreflex drive and active expiration in chronic heart failure rats. (a) representative traces of one rat per group showing tidal volume (V_T) and respiratory frequency (Rf) at rest and during central chemoreflex stimulation with hypercapnia (F_iCO_2 7%) measured by unrestrained whole-body plethysmography. (b,c) quantification of central chemoreflex sensitivity in Sham control rats and CHF rats treated with vehicle or SSP immunotoxin, (b) measurement of minute ventilation (V_E) in hypercapnia vs. normocapnia and (c) hypercapnic ventilatory response (HCVR). (d) representative traces of ventilation showing the early (E1) and late expiratory (E2) phases. (e) measurement of active expiration as the late-to-early (E2/E1) expiratory ratio. (f) representative images of histological sections (30 μm) of the ventral surface of the brainstem of rats receiving SSP toxin or vehicle (0.9% NaCl) in the RTN (scale bar 200 μm). (g) quantification of the total number of RTN chemosensory neurons (Phox2b$^+$ TH$^-$ phenotype) in Sham control rats and CHF rats treated with Vehicle or with the SSP toxin. Data show mean $\pm$ s.e.m.; Data was analysed using one-way ANOVA; *: p<0.05 vs. Sham+Veh; +: p<0.05 vs. CHF+Veh; #: p<0.05 vs. Sham+SSP). n=8 animals per group.

neuroplasticity in the RTN modulates synaptic strength and respiratory network excitability in response to elevated CO_2 (i.e. natural stimuli).[47] Here, repetitive RTN photo-stimulation in healthy rats mimics multiple effects of abnormally elevated P_aCO_2 levels (i.e., oscillatory breathing, hypopneas) supporting our results (Figure 2) demonstrating the importance of the RTN to the generation of disordered breathing.

RTN drives breathing disorders in heart failure via an astrocyte-dependent mechanism

Considering that CHF rats showed a higher prevalence of breathing disorders and that these were dependent on RTN chemoreceptor neurones, we aimed to determine if these neurons display molecular characteristics of increased neuronal activity (Figure S3a). Using immunoblot, we observed that CHF animals showed similar ΔFosB protein expression in RTN micro punches compared to control rats suggesting no chronic RTN neuronal activation in CHF (Figure 4a). Since RTN astrocytes can regulate neuronal function through synaptic and non-synaptic modulation,[14,15,48] we

determined in the same RTN samples, the activity of astrocytes residing within the RTN. Immunoblot analyses showed that CHF rats display a ~40% decrease in the expression levels of the glial fibrillary acidic protein (GFAP) compared to control rats, with no changes in glial cell density as noted by similar expression of S100B protein in CHF and control (Figure 4b,c). These results strongly suggest that RTN astrocytes may undergo metabolic inhibition in CHF. Previous evidence indicates that CO_2/H^+-evoked activation of RTN astrocytes results in ATP release.[11] Using a quantitative bioluminescence assay, we determined the bioavailability of ATP within the RTN in CHF rats. ATP levels were significantly lower in CHF compared to control (Figure 4d). Furthermore, ATP levels were positively correlated with astrocyte metabolic activity in the RTN (Figure S3c). Therefore, we hypothesized that inhibition of RTN astrocytes may play a role in the development of disordered breathing during CHF. An adeno-associated virus (AAV) containing an excitatory designer receptor exclusively activated by designer drugs (DREADDs; hM3Dq) under the control of GFAP promoter was bilaterally injected into the RTN of CHF rats (CHF
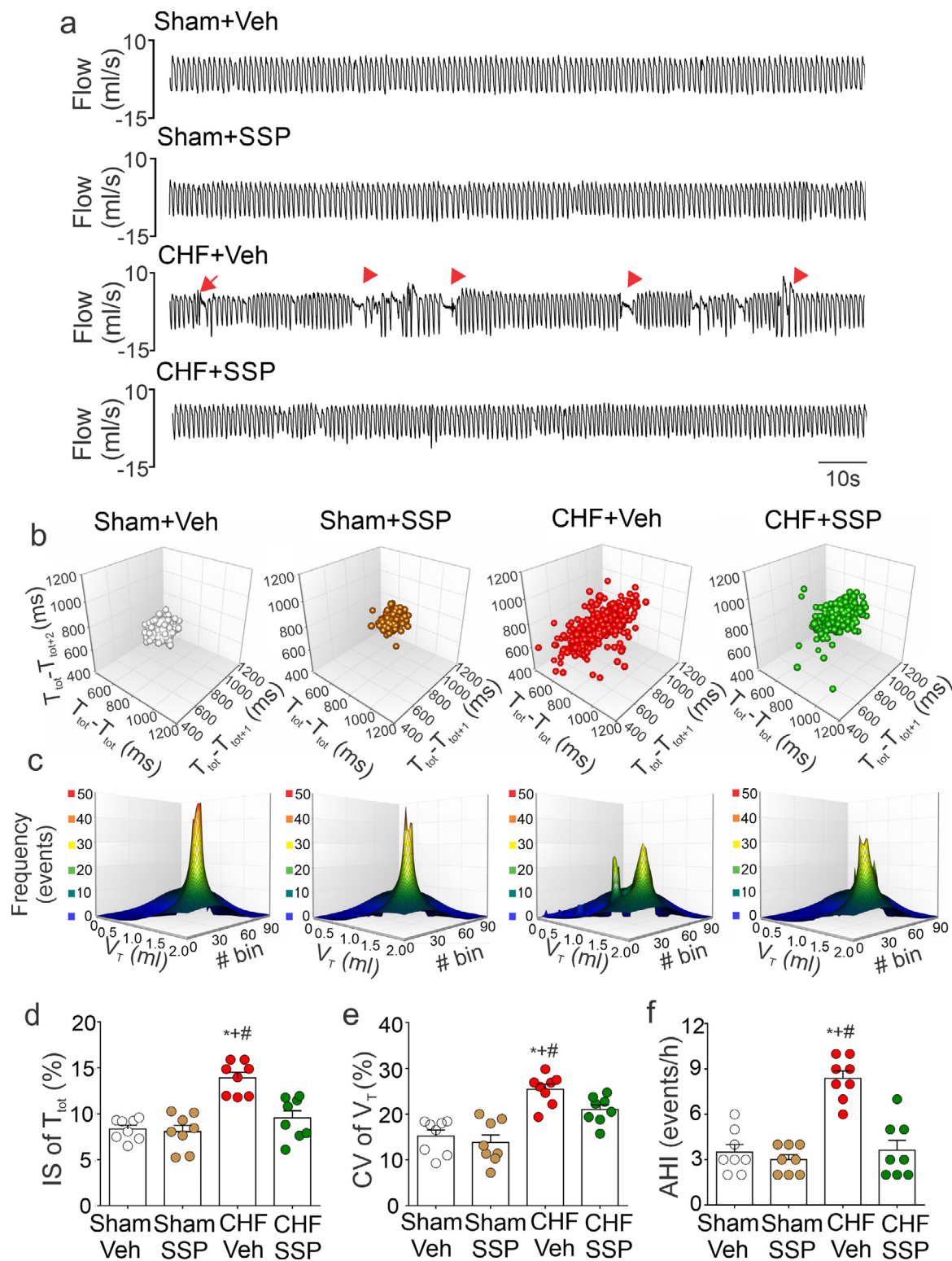
Figure 2. Partial RTN neurones ablation in chronic heart failure rats improve resting breathing pattern. (a), representative traces of resting ventilation in one rat per group. Arrowheads highlight respiratory disorders such as apnoeas and hypopneas. (b,c) representative plots of ventilatory variability in one rat per group. (B) Poincaré plots showing breath-to-breath T_{TOT} variability. (c) histograms of V_T cycle amplitudes. (d-f) measurements of respiratory instability during resting ventilation. (d) irregularity score (IS), (e) coefficient of variation of V_T respiratory cycles, (f) apnoea-hypopnea index (AHI). Data show mean $\pm$ s.e.m.; Data was analysed using one-way ANOVA; *: $p<0.05$ vs. Sham+Veh, +: $p<0.05$ vs. CHF+Veh; #: $p<0.05$ vs. Sham+SSP). n=8 animals per group.
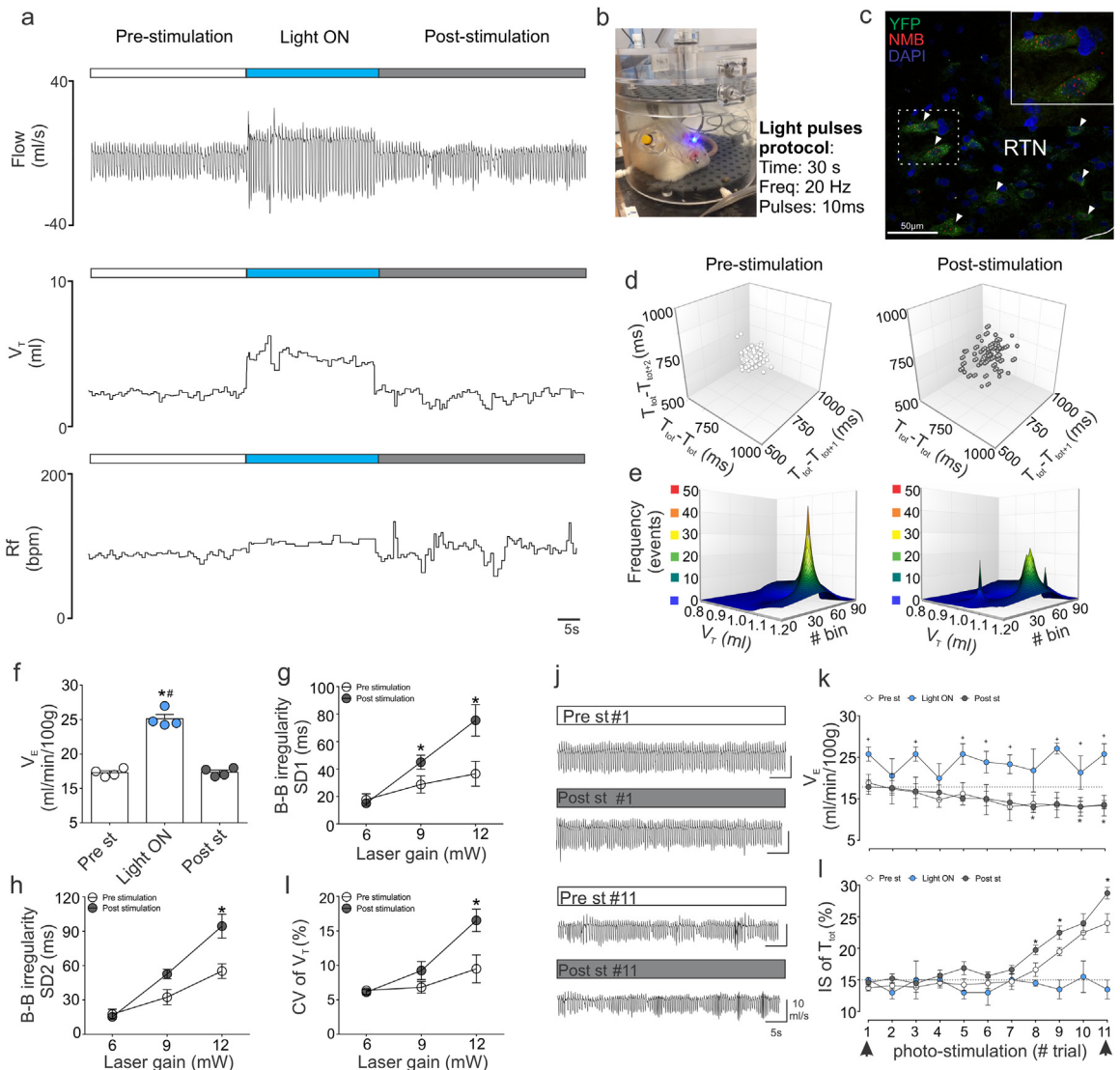
Figure 3. Repetitive optogenetic photo-stimulation of RTN neurons elicits breathing disorders. (a) representative traces of ventilatory flow, respiratory frequency (Rf) and tidal volume (V_T) at rest, before, during and after unilateral high frequency photo-stimulation of RTN neurons measured by unrestrained whole-body plethysmography (460 nm, 30 s trains of 10 ms pulses delivered at 20 Hz spaced by 6 min during 1 h). (b) representative picture of one rat during optogenetic stimulation. (c) Neuromedin B positive neurons within the RTN co-localized with channelrhodopsin2 (ChR2). RTN neurons were transduced *in-vivo* with a lentiviral vector to express ChR2 (LVV-PRSX8-ChR2-YFP). RNAscope against neuromedin B (Nmb) revealed that YFP^+ cells within the RTN co-express Nmb, a biomarker of RTN chemoreceptor neurons (scale bar 50 μm). (d,e) representative plots of ventilatory variability before and after optogenetic RTN photo-stimulation. (d) Poincare plots showing breath-to-breath variability. (e) histograms of V_T cycle amplitudes. (f) minute ventilation (V_E) during photo-stimulation. (g-i) quantification of ventilatory variability parameters at different laser gains during the experimental protocol. (g) short-term variability (SD1) and long-term variability (SD2, h) of breath-to-breath variability. (i) coefficient of variation of V_T, (j) representative traces of ventilation during the first and last train of light pulse stimulation (pre and post light ON). (k) quantification of V_E and (l) irregularity score (IS) before (∼200 breaths), during (∼50 breaths) and after (∼200 breaths) photo-stimulation. Data show mean ± s.e.m.; Data was analyzed using one-way analysis of variance (ANOVA) (f-i: *: $p < 0.05$ vs. Pre-stimulation, #: $p < 0.05$ vs. post-stimulation) and paired t-test (k, *: $p < 0.05$ vs. baseline, +: $p < 0.05$ vs. Pre-stimulation; l, *: $p < 0.05$ vs. Pre-stimulation). n=4 animals.

+DREADD$_{Gq}$) for chronic astrocyte chemo-genetic activation (Figure S3b). Compared to CHF rats injected with an empty vector (CHF+Ctrl), long-term activation of RTN astrocytes (4 weeks) using clozapine-n-oxide (CNO) in CHF+DREADD$_{Gq}$ rats did not change the ventilatory response to hypercapnia (Figures 4e−g; S3e,

f) nor eupnoeic baseline ventilatory and cardiac parameters (Supplementary Tables 4 and 5). In contrast, disordered breathing in CHF was abrogated by long-term stimulation of RTN astrocytes. As shown in Figure 4, breathing rate and amplitude were both significantly improved in CHF+DREADD$_{Gq}$ rats (Figure 4h-l). The incidence of apnoeas/hypopneas were also reduced by chronic activation of RTN astrocytes using DREADD$_{Gq}$ in CHF rats (Figure 4q; Supplementary Table 6). As shown in Figure 4m, DREADD$_{Gq}$ expression was exclusively targeted to GFAP positive cells within the RTN (-11.6 caudal to bregma). As expected, long-term activation of DREADD$_{Gq}$ in the RTN induced the recovery of GFAP levels in CHF rats along with increases in ATP levels (Figure 4n−p). Importantly, recovery of ATP bio-availability in the RTN of CHF rats that underwent chemo-genetic astrocyte activation was significantly associated with decreases in AHI (Figure S3g). Also, activation of RTN astrocytes did not further exacerbate the heightened hypercapnic ventilatory response observed in CHF rats. In contrast, we found that activation of RTN astrocytes is closely linked to increases in hypercapnic ventilatory response in Sham rats (Figure S3d). Together these results support that notion that RTN astrocytes and astrocyte-mediated ATP signalling play a fundamental role in regulating resting breathing in CHF and that decreases in RTN astrocyte activity in CHF play a role in the development of breathing disorders.

Reduced P2X7 receptor expression in the RTN promotes irregular breathing in heart failure

Astrocytes represent the major source of purinergic drive in the RTN under normal conditions.[16,17] It has been shown that P2X7 receptor (P2X7r)-mediated ATP release amplifies intracellular Ca^{2+} signalling in astrocyte cell cultures from the spinal cord[49] and this mechanism serves as a main substrate to maintain synaptic network activity.[50] Accordingly, to test whether the P2X7r may participate in the astrocyte-driven breathing disorders in the pathophysiology of CHF, we first analysed mRNA and protein expression levels of the P2X7r in the RTN. Compared to control rats, CHF animals showed a significant reduction in P2X7r expression at both transcript and protein levels (Figure 5a,b). Next, using RNAscope multiplex *in situ* hybridization, we confirmed that P2X7r mRNA co-localized with GFAP positive cells in the RTN (Figure 5c), supporting the notion that P2X7r within RTN astrocytes could participate in purinergic signalling and consequently in breathing regulation (Figure 5d). The contribution of the P2X7r to respiratory physiology has not been previously explored, therefore, to determine if the P2X7r plays a role in regulation of breathing we first studied ventilation in P2X7r knock-out mice (P2X7r$^{-/-}$). Interestingly, both wild type (WT) and P2X7r$^{-/-}$ mice showed nearly identical

central chemoreflex gain (Figures 5e,f; S4b,c), but P2X7r$^{-/-}$ mice exhibited a slight decrease in resting minute ventilation compared to WT mice (Supplementary Table 7). These results agree with previous reports showing that purinergic signalling can modulate RTN chemoreflex function but does not mediate chemoreceptor neuron pH sensitivity.[51] In contrast to our chemoreflex findings, we observed irregular breathing patterns at rest in P2X7r$^{-/-}$ mice compared to WT mice. Figure 4g illustrates the loss of ventilatory stability and the increases in apnoea incidence observed in the P2X7r$^{-/-}$ mutant mice. Poincare plots from P2X7r$^{-/-}$ mice showed wide dispersion of the breath-to-breath intervals and non-symmetrical distribution of V_T amplitudes compared to WT mice (Figure 5h,i). Accordingly, both SD1 and SD2 breath to breath (B-B) interval variability indexes, and the coefficient of variation of V_T were both markedly augmented in P2X7r$^{-/-}$ mice compared to WT age-matched controls (Figure 5J−L). AHI was also higher in P2X7r$^{-/-}$ mice compared to WT mice (Figure 5M). Next, in order to test how much of these effects were attributable to P2X7r deficiency within the RTN, we selectively over-expressed the P2X7r in RTN astrocytes from P2X7r$^{-/-}$ mice. For this, AAV5 constructs containing the P2X7r gene under the control of GFAP promoter were injected bilaterally into the RTN of P2X7r$^{-/-}$ mice (P2X7r$^{-/-}$+AVV$_{P2X7r}$) (Figure S4a). Selective restoration of P2Xr expression into RTN astrocytes had no effects on the hypercapnic ventilatory response (Figure 5e,f) but markedly improved breathing pattern regularity in the P2X7r$^{-/-}$ mice and decreased the incidence of apnoeic episodes (Figure 5g−m). Together, these data unveil a novel role of the astrocyte P2X7r in RTN-mediated respiratory rhythm regulation.

RTN-targeted restoration of the P2X7r expression abolishes disordered breathing in heart failure

Since downregulation/lack of P2X7r in RTN astrocytes was associated with reductions in ATP availability and the development of breathing disorders in healthy rodents, and since CHF rats showed reduced astrocyte P2X7r expression and irregular breathing, we aimed to determine the potential salutary effect of cell-targeted increases in P2X7r expression on the incidence of breathing disorders in rats with CHF. Accordingly, we bilaterally injected an empty viral vector or viral vector expressing the P2X7r under GFAP promoter (Figure S5a) into the RTN of CHF rats. Increasing the expression of the P2X7r within RTN astrocytes of CHF rats (CHF+P2X7r) did not significantly change central chemoreflex gain (Figures 6a,b and S5c,d) but produced a slight rise in minute ventilation in normoxia (Supplementary Table 10). Remarkably, the hallmark irregular resting breathing patterns observed in CHF rats were
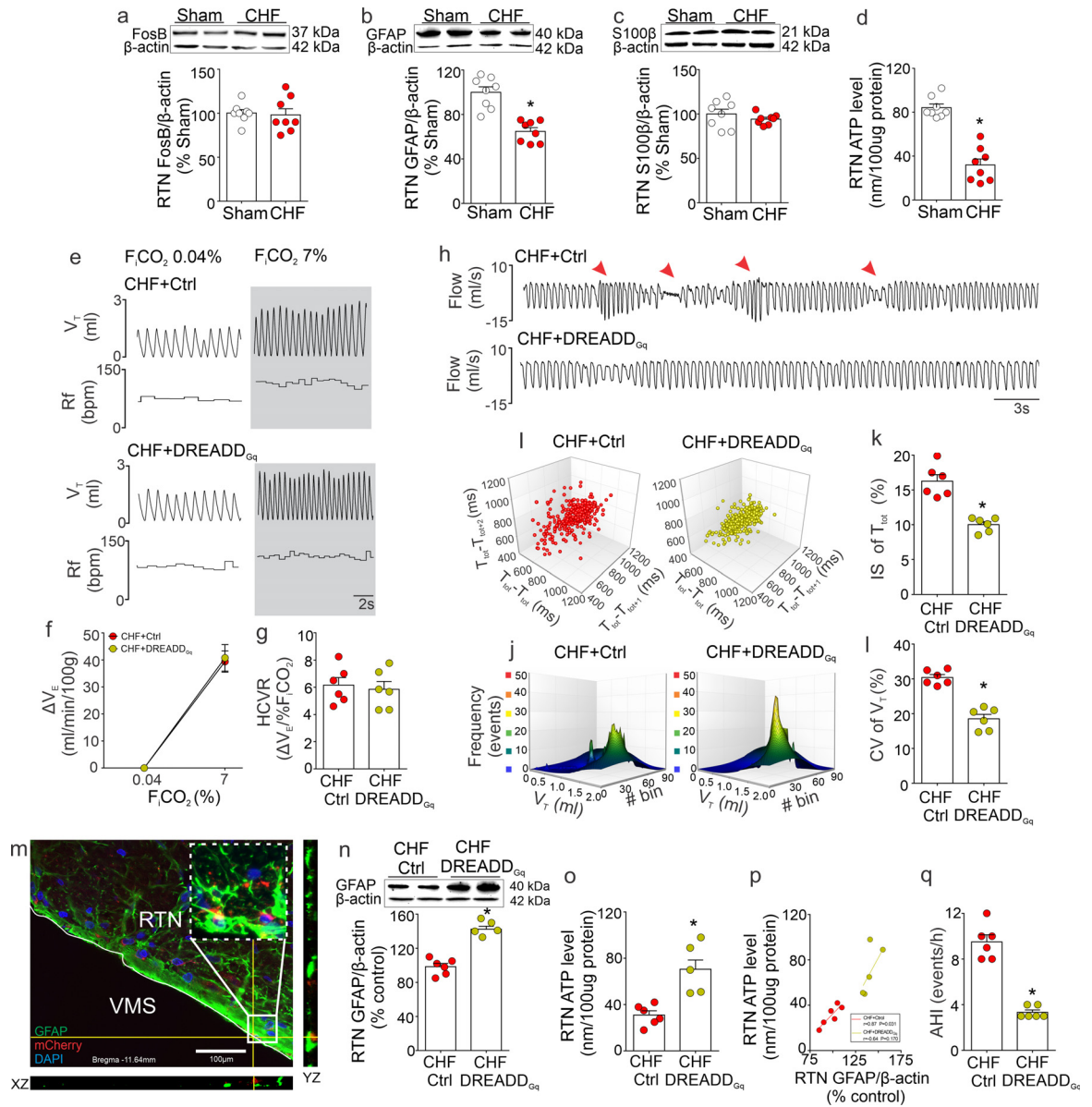
Figure 4. Contribution of RTN astrocytes to breathing disorders in heart failure. (a) RTN relative protein expression levels of FosB, Glial fibrillary acidic protein (GFAP, b) and $S100\beta$ (c) in Sham rats (n=8) and CHF rats (n=8). (d) measurements of RTN ATP levels in Sham and CHF rats. (e) representative traces of V_T and Rf at rest and during central chemoreflex stimulation by hypercapnia (F_iCO_2 7%) in CHF rats transfected with an excitatory Designer Receptors Exclusively Activated by Designer Drugs (CHF+DREADD$_{Gq}$, n=6) and control empty vector (CHF+Ctrl, n=6) following chronic (for 2 weeks) DREADD activation with clozapine-N-oxide (CNO). (f,g) quantification of central chemoreflex sensitivity in CHF+Ctrl and CHF+DREADD$_{Gq}$ rats, (f) the difference in minute ventilation (V_E) in hypercapnia vs. baseline ventilation and (g) the hypercapnic ventilatory response (HCVR). (h) representative traces of ventilation of one CHF+Ctrl and one CHF+DREADD$_{Gq}$ rat. Arrowheads showing apnoeas and hypopnoes. (i,j), representative plots of ventilatory variability at rest. (I) Poincare plots showing breath-to-breath T_{TOT} variability. (j) histograms of V_T. (k-m) measurements of respiratory instability during resting ventilation. (k), irregularity score (IS), (l), coefficient of variation of V_T. (m) histological confirmation of RTN astrocytic viral transfection of the excitatory DREADD (mCherry fluorescence) (scale bar 100 μm). (n) western blots experiments showing relative GFAP protein levels in the RTN of CHF+Ctrl (n=6) and CHF+DREADD$_{Gq}$ rats (n=5). (o) measurement of RTN ATP levels. (p) Correlation analysis between GFAP expression and ATP levels. (q) apnoea-hypopnea index (AHI) Data show mean ± s.e.m.; Data was analysed using unpaired t-tests (a-d *: p<0.05 vs. Sham; e-q *: p<0.05 vs. CHF+Ctrl). (a-d).
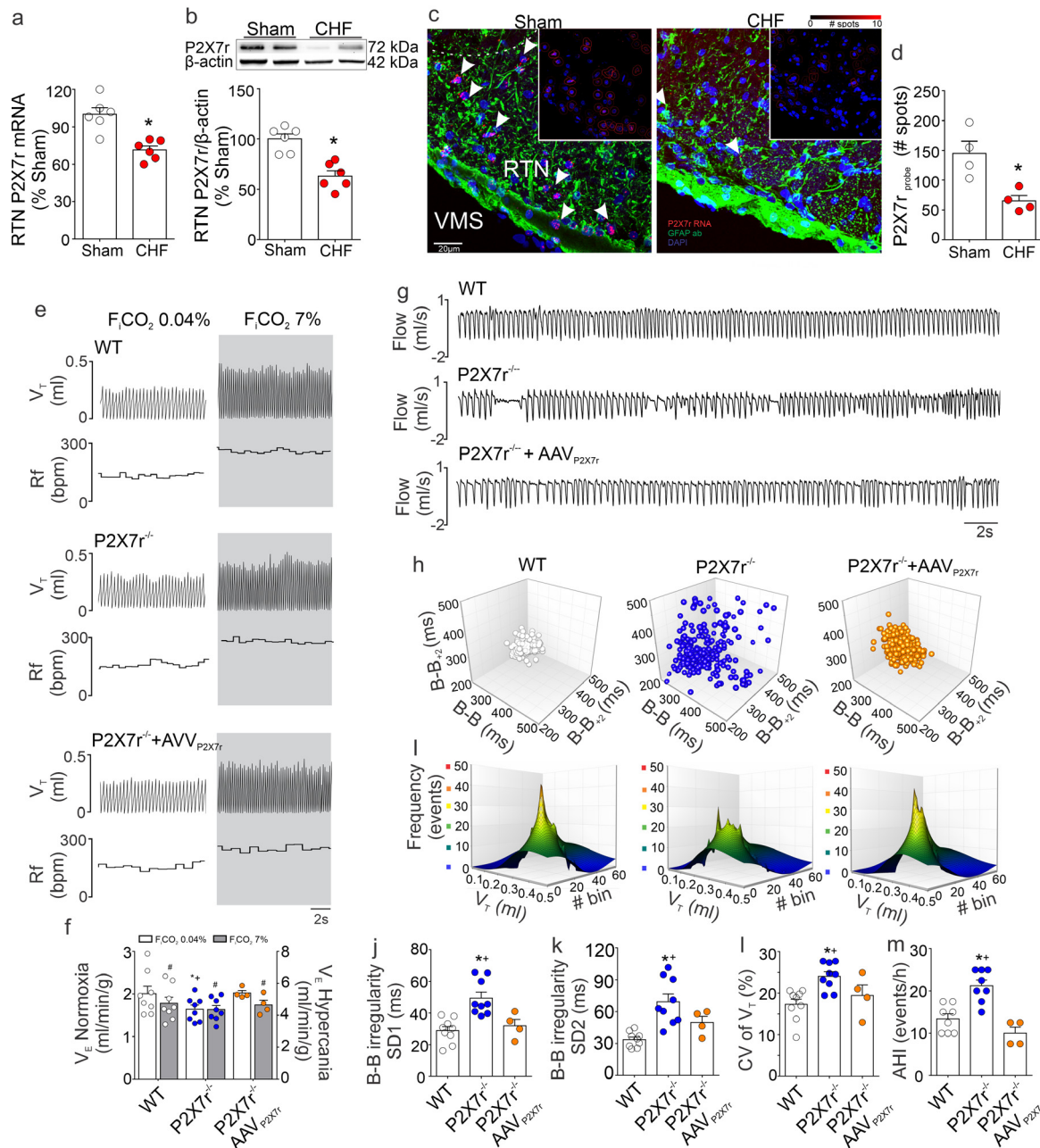
Figure 5. Lack of P2X7r in the RTN is linked to disordered breathing. (a) relative P2X7r mRNA and (b) protein expression in Sham control rats (n=6) and CHF rats (n=6) by qPCR and western blot, respectively. (c) representative image of astrocytic P2X7r mRNA immunolabelling in brainstem sections containing the RTN in one Sham and CHF rat (scale bar 20 μm). (d) quantification of P2X7r RNA spots detected (e) representative traces of V_T and Rf in one wild-type mouse (WT; n=9), P2X7r KO mouse (P2X7r$^{-/-}$; n=9) and one KO mouse transfected with an adenoviral vector expressing the P2X7 receptor (P2X7r$^{-/-}$+AAV$_{P2X7r}$ n=4) into the RTN at baseline normoxic conditions and during hypercapnic stimulation. (f) measurements of V_E at baseline and during hypercapnia (F_iCO_2 7%) in WT, P2X7r$^{-/-}$ and P2X7r$^{-/-}$+AAV$_{P2X7r}$ mice. (g) representative traces of resting ventilation in one WT, P2X7r$^{-/-}$ and P2X7r$^{-/-}$+ AAV$_{P2X7r}$ mouse. (h-i), representative plots of ventilatory variability at rest. (h) Poincare plots showing breath-to-breath variability. (i) histograms of V_T. (j-m) measurements of respiratory instability during resting ventilation in all experimental groups. (j-k) SD1 and SD2 of the breath-to-breath variability, respectively, (l) coefficient of variation of V_T cycle amplitudes, (m) apnoea-hypopnea index (AHI). Data show mean ± s.e.m.; Data was analyzed using unpaired t-tests (a,b, *: $p<0.05$ vs. Sham), two-way ANOVA (f, #: $p<0.05$ vs. its own V_E in baseline) and one-way ANOVA (g-m, *: $p<0-05$ vs. WT, +: $p<0.05$ vs. P2X7r$^{-/-}$+ AAV$_{P2X7r}$).

completely normalized by restoration of P2X7r expression in RTN astrocytes of CHF+P2X7r rats (Fig 6c−h, Supplementary Table 11). In addition, RTN ATP bioavailability was augmented by P2X7r overexpression in CHF rats (Figure 6i−k). Together, these results strongly support the notion that RTN astrocytes play a pivotal role in the generation/maintenance of disordered breathing in CHF through a P2X7r-dependent mechanism.

Discussion

Irregular breathing patterns, including apnoeas/hypopneas and oscillatory breathing are highly prevalent in several diseases. However, the mechanisms underlying dysregulation of respiratory control are not fully known. Unstable breathing varies with changes in chemoreceptor activity through mechanism involving CO_2-induced central instability.[52−54] Interestingly, astrocytes residing within brainstem chemoreceptor areas are capable of regulate breathing through ATP release.[11,55] Here we show that the lack of P2X7r selectively expressed in astrocyte of the RTN, a main source for brain chemoreception that controls respiratory chemoreflex drive, trigger irregular breathing. In addition, using experimental CHF rats, a disease characterized by breathing irregularities, we found that astrocyte activity, ATP levels and P2X7r gene and protein expression were all reduced in the RTN. Importantly, chronic chemogenetic activation of RTN astrocytes in CHF increased ATP levels and improve breathing pattern regularity. Finally, increasing the expression of P2X7r only in RTN astrocytes markedly reduced apnoea incidence and oscillatory breathing in both CHF rats and P2X7r$^{-/-}$ knockout mice. Our results support that the RTN contribute to the maintenance of irregular breathing and that RTN astrocytes play a pivotal role on breathing pattern regulation by a mechanism encompassing ATP release and the P2X7r.

The cellular mechanisms that underlie irregular breathing patterns in CHF are poorly understood. Chemoreceptors play a major role in the ventilatory adjustments to hypercapnia/hypoxia[56] but their influence on resting breathing, particularly when they are disrupted (as in CHF) is not yet completely understood. Central chemoreceptor neurones in the RTN are key players in the regulation of the CO_2-mediated central ventilatory drive.[8] The present study confirms previous reports showing that RTN chemoreceptor neurones regulate ventilation in hypercapnia and extends these findings with new and comprehensive evidence showing that repetitive stimulation of RTN chemoreceptor neurons triggers ventilatory plasticity leading to irregular oscillatory breathing.[18] Identifying all of the mechanisms underpinning the effects of RTN stimulation on respiratory rhythm is outside of the scope of the present study, but it is plausible that repetitive stimulation of RTN chemoreceptor neurones results in anomalous afferent neural input (i.e. asynchronous) to the respiratory pattern generator.[9] It has been proposed that in pathophysiological contexts characterized by breathing disorders (e.g., CHF), alterations in RTN-mediated chemoreflex function induces instability in the respiratory control network, fostering a feed-forward mechanism that perpetuates breathing irregularity.[8,57] It is worth noting that no specific cellular or molecular mechanisms have been identified as putative pathways involved in RTN chemoreceptor-mediated disordered breathing. Previous studies have shown that astrocytes residing within the RTN modulate chemoreceptor neurones through the release of one or more gliotransmitters that regulate chemoreceptor neurones function.[11,14,16] In the present study we provide compelling evidence that RTN astrocytes play an important role in oscillatory breathing in CHF. Our data shows that reduced activity of astrocytes in CHF is accompanied by decreased levels of ATP, a well-known gliotransmitter, and that increasing astrocyte activity using an excitatory DREADD$_{Gq}$ not only increases ATP bioavailability but also normalizes disordered breathing in CHF rats. Deciphering whether this effect is the consequence of the direct actions of ATP and/or related purines on RTN chemoreceptor neurones, or alternatively, an autocrine effect of ATP on RTN astrocytes to further facilitate the release of another gliotransmitter is outside the scope of present study and remains to be determined. However, it has been shown that purinergic modulation of RTN neurones depends on the propagation of Ca^{2+} waves coming from ventral surface astrocytes, possibly by the activation of Ca^{2+}-permeable P2X channels present on the astrocyte cell surface[55]. Indeed, elegant experiments performed by Gourine, and colleagues demonstrated that increases in medullary astrocyte activity results in a Ca^{2+}-dependent ATP release in micromolar amounts.[11,12,55] Interestingly, among the P2X receptor family, the P2X7 receptor is preferentially expressed in glial cells and displays activity-dependent allosteric regulation through Ca^{2+}-calmodulin.[58] Furthermore, low micromolar concentrations of ATP activate P2X7r increasing its open probability and cationic conductance.[59] The latter also leads to pannexin 1 recruitment to form an active heterodimer complex (P2X7r-pannexin1) that is responsible for ATP release.[60] Thus, the P2X7r is a promissory candidate to modulate ATP release within the RTN. Our study shows that P2X7r is constitutively expressed in RTN astrocytes and that deletion in P2X7r$^{-/-}$ mice results in irregular resting breathing patterns that are reversed by selective RTN astrocyte-targeted expression of the P2X7r. We validated these findings using a pathologically relevant model characterized by disordered breathing (i.e., CHF) in which we show for the first time that CHF rats have reduced expression of P2X7r in the RTN and that viral transfection of the P2X7r into RTN astrocytes completely restores normal breathing patterns in CHF rats.
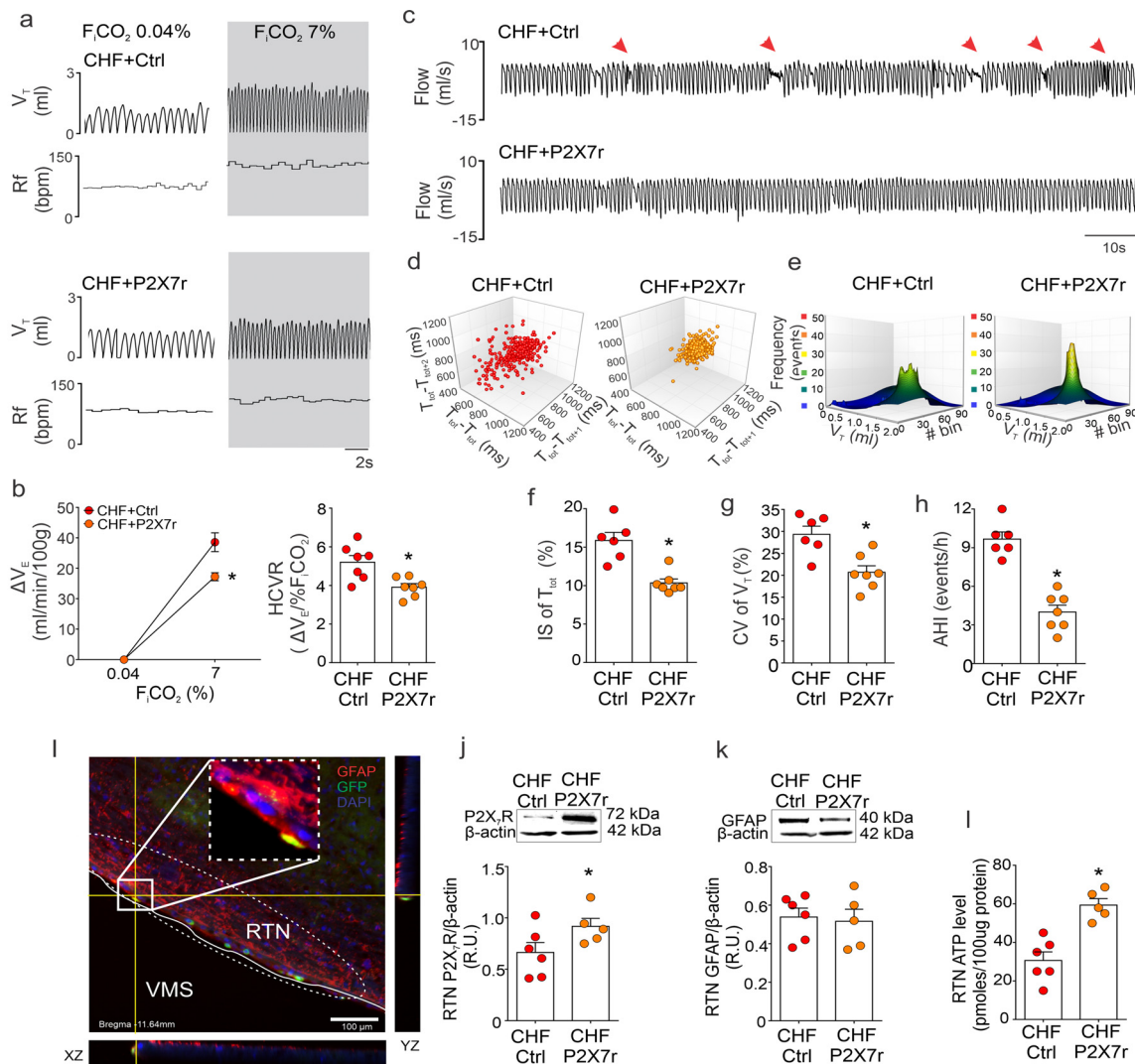
Figure 6. P2X7r upregulation in RTN astrocytes restores normal breathing patterns in heart failure. (a) representative traces of one CHF+Ctrl and one CHF rat after transfection with AAV5- GFAP-P2X7r-P2A-GFP (CHF+P2X7r) showing tidal volume (V_T) and respiratory frequency (Rf) at rest and during central chemoreflex stimulation with hypercapnia (F_iCO_2 7%). (b) quantification of V_E at baseline and during central chemoreceptor stimulation with hypercapnia. (c) representative traces of resting ventilation obtained in one CHF+Ctrl rat and one CHF+P2X7r rat. Arrowheads shows breathing disorders. (d,e) representative plots of ventilatory variability at rest in one CHF+Ctrl rat (n=7) and one CHF+P2X7r rat (n=7) . (d) Poincare plots showing breath-to-breath T_{TOT} variability. (e) histograms of V_T. (f,h) measurements of respiratory instability during resting ventilation in the 2 groups. (f) irregularity score (IS), (g) coefficient of variation of V_T, (h) apnoea-hypopnea index (AHI). (i) visual confirmation of astrocytic viral transfection in the RTN by GFP fluorescence and GFAP immunolabeling (scale bar 100 μm). (j-k), relative protein expression levels of the P2X7r (j) and GFAP (k) in RTN micro-punches. (l) quantification of RTN ATP levels. Data show mean ± s.e.m.; Data was analysed using unpaired t-tests (c-l *: p<0.05 vs. CHF+Ctrl).

Several limitations are inherent in our study. First, our study was not oriented to provide anatomical landmarks for each stereotaxic approximation (i.e. ablation, optogenetic and/or chemogenetic experiments) targeting the RTN. Then, physiological data and cell count/immunolocalization served as proof of success of our experimental approaches. Specifically, we counted RTN phox2b positive neurons devoid of TH staining (classical phenotype of RTN chemoreceptor neurons described elsewhere in the literature) within the ventral aspect of the medulla and reported fewer RTN phox2b neurons following stereotaxic injection of SSP-saporin toxin. Using the exact same stereotaxic coordinates, we found that optogenetic stimulation of this area triggers the classic ventilatory response elicited by activation of RTN neurons. Accordingly, both our immunohistochemical and physiological data strongly

support that we effectively target the RTN region. Second, we showed that normalizing RTN astrocyte activity and/or the restoration of the P2X7r expression within RTN astrocytes significantly improved breathing function in CHF rats. However, this study was not focused on the study of other pathological hallmarks of CHF. Indeed, the effects of our interventions on neurohumoral activation (that take place in CHF and has been suggested to be partially regulated by the chemoreflex pathway) was not tested. Then, future studies are needed to show any potential beneficial effect of normalizing RTN function on neurohumoral activation in the setting of CHF. Lastly, the relative short-term of our experiments targeting RTN astrocytes did not allow us to fully unveil the therapeutic potential of our interventions on CHF progression. Further studies should focus on the effects of restoring RTN function on disease progression.

In summary, astrocytic P2X7r within the RTN plays a role in respiratory rhythm regulation and may be a promising candidate for the treatment of respiratory disorders in CHF. Whether targeting the P2X7r may help improve breathing in other pathological conditions is an exciting topic that deserves further investigation.

Contributors
C.T, D.C.A, H.S.D, E.D.J., performed the experiments and analysed and interpreted the data. CT performed all experiments in animals with the assistance of D.C.A and E.D.J. (rats) and H.S.D and E.D.J (mice). K.G.S., K.V.P., A.L.H., and A.R.G. participated in experimental procedures (RNAscope, western blots, qPCR, ATP measurements), analysed and interpreted the data. T.S.M., A.C.T, participated in experimental procedures (immunofluorescence and imaging) and manuscript revision. N.J.M. contributed to manuscript preparation and revision, and R.D.R designed experiments, approved experimental protocols, and wrote the manuscript with input from CT. All authors have read and approved the final manuscript.

Declaration of interests
The authors have declared that no conflict of interest exists.

Data Sharing statement
The datasets used and/or analysed during the current study available from the corresponding author on reasonable request.

Supplementary materials
Supplementary material associated with this article can be found in the online version at doi:10.1016/j.ebiom.2022.104044.

References
1 Parati G, Lombardi C, Castagna F, et al. Heart failure and sleep disorders. *Nat Rev Cardiol*. 2016;13(7):389–403.
2 Giannoni A, Emdin M, Bramanti F, et al. Combined increased chemosensitivity to hypoxia and hypercapnia as a prognosticator in heart failure. *J Am Coll Cardiol*. 2009;53(21):1975–1980.
3 Narkiewicz K, Pesek CA, van de Borne PJ, Kato M, Somers VK. Enhanced sympathetic and ventilatory responses to central chemoreflex activation in heart failure. *Circulation*. 1999;100(3):262–267.
4 Hanly P, Zuberi N, Gray R. Pathogenesis of Cheyne-Stokes respiration in patients with congestive heart failure. Relationship to arterial PCO_2. *Chest*. 1993;104(4):1079–1084.
5 Nogues MA, Benarroch E. Abnormalities of respiratory control and the respiratory motor unit. *Neurologist*. 2008;14(5):273–288.
6 Del Negro CA, Funk GD, Feldman JL. Breathing matters. *Nat Rev Neurosci*. 2018;19(6):351–367.
7 Nattie E, Li A. Central chemoreceptors: locations and functions. *Compr Physiol*. 2012;2(1):221–254.
8 Guyenet PG, Stornetta RL, Souza G, Abbott SBG, Shi Y, Bayliss DA. The retrotrapezoid nucleus: central chemoreceptor and regulator of breathing automaticity. *Trends Neurosci*. 2019;42(11):807–824.
9 Moreira TS, Sobrinho CR, Falquetto B, et al. The retrotrapezoid nucleus and the neuromodulation of breathing. *J Neurophysiol*. 2021;125(3):699–719.
10 Kumar NN, Velic A, Soliz J, et al. Regulation of breathing by CO_2 requires the proton-activated receptor GPR4 in retrotrapezoid nucleus neurons. *Science*. 2015;348(6240):1255–1260.
11 Gourine AV, Kasymov V, Marina N, et al. Astrocytes control breathing through pH-dependent release of ATP. *Science*. 2010;329(5991):571–575.
12 Sheikhbahaei S, Turovsky EA, Hosford PS, et al. Astrocytes modulate brainstem respiratory rhythm-generating circuits and determine exercise capacity. *Nat Commun*. 2018;9(1):370.
13 Rajani V, Zhang Y, Jalubula V, et al. Release of ATP by pre-Botzinger complex astrocytes contributes to the hypoxic ventilatory response via a Ca^{2+}-dependent P2Y1 receptor mechanism. *J Physiol*. 2018;596(15):3245–3269.
14 Mulkey DK, Wenker IC. Astrocyte chemoreceptors: mechanisms of H+ sensing by astrocytes in the retrotrapezoid nucleus and their possible contribution to respiratory drive. *Exp Physiol*. 2011;96(4):400–406.
15 Turovsky E, Theparambil SM, Kasymov V, et al. Mechanisms of CO2/H+ Sensitivity of Astrocytes. *J Neurosci*. 2016;36(42):10750–10758.
16 Wenker IC, Sobrinho CR, Takakura AC, Moreira TS, Mulkey DK. Regulation of ventral surface CO_2/H^+-sensitive neurons by purinergic signalling. *J Physiol*. 2012;590(9):2137–2150.
17 Barna BF, Takakura AC, Mulkey DK, Moreira TS. Purinergic receptor blockade in the retrotrapezoid nucleus attenuates the respiratory chemoreflexes in awake rats. *Acta Physiol (Oxf)*. 2016;217(1):80–93.
18 Diaz HS, Andrade DC, Toledo C, et al. Episodic stimulation of central chemoreceptor neurons elicits disordered breathing and autonomic dysfunction in volume overload heart failure. *Am J Physiol Lung Cell Mol Physiol*. 2020;318(1):L27–L40.
19 Rudzinski E, Kapur RP. PHOX2B immunolocalization of the candidate human retrotrapezoid nucleus. *Pediatr Dev Pathol*. 2010;13(4):291–299.
20 Levy J, Droz-Bartholet F, Achour M, Facchinetti P, Parratte B, Giuliano F. Parafacial neurons in the human brainstem express specific markers for neurons of the retrotrapezoid nucleus. *J Comp Neurol*. 2021;529(13):3313–3320.
21 Marina N, Tang F, Figueiredo M, et al. Purinergic signalling in the rostral ventro-lateral medulla controls sympathetic drive and contributes to the progression of heart failure following myocardial infarction in rats. *Basic Res Cardiol*. 2013;108(1):317.
22 Toledo C, Lucero C, Andrade DC, et al. Cognitive impairment in heart failure is associated with altered Wnt signaling in the hippocampus. *Aging (Albany NY)*. 2019;11(16):5924–5942.

23 Toledo C, Andrade DC, Lucero C, et al. Cardiac diastolic and autonomic dysfunction are aggravated by central chemoreflex activation in heart failure with preserved ejection fraction rats. *J Physiol.* 2017;595(8):2479–2495.

24 Diaz HS, Andrade DC, Toledo C, et al. Inhibition of brainstem endoplasmic reticulum stress rescues cardiorespiratory dysfunction in high output heart failure. *Hypertension.* 2021;77(2):718–728.

25 Andrade DC, Toledo C, Diaz HS, et al. Ablation of brainstem C1 neurons improves cardiac function in volume overload heart failure. *Clin Sci (Lond).* 2019;133(3):393–405.

26 Toledo C, Andrade DC, Diaz HS, et al. Rostral ventrolateral medullary catecholaminergic neurones mediate irregular breathing pattern in volume overload heart failure rats. *J Physiol.* 2019;597 (24):5799–5820.

27 Takakura AC, Barna BF, Cruz JC, Colombari E, Moreira TS. Phox2b-expressing retrotrapezoid neurons and the integration of central and peripheral chemosensory control of breathing in conscious rats. *Exp Physiol.* 2014;99(3):571–585.

28 Souza G, Stornetta RL, Stornetta DS, Abbott SBG, Guyenet PG. Contribution of the retrotrapezoid nucleus and carotid bodies to hypercapnia- and hypoxia-induced arousal from sleep. *J Neurosci.* 2019;39(49):9725–9737.

29 Paxinos G, Watson C. *The Rat Brain in Stereotaxic Coordinates: Hard Cover Edition.* Elsevier; 2006.

30 Holloway BB, Viar KE, Stornetta RL, Guyenet PG. The retrotrapezoid nucleus stimulates breathing by releasing glutamate in adult conscious mice. *Eur J Neurosci.* 2015;42(6):2271–2282.

31 Abbott SB, Stornetta RL, Fortuna MG, et al. Photostimulation of retrotrapezoid nucleus phox2b-expressing neurons in vivo produces long-lasting activation of breathing in rats. *J Neurosci.* 2009;29 (18):5806–5819.

32 Chen N, Sugihara H, Kim J, et al. Direct modulation of GFAP-expressing glia in the arcuate nucleus bi-directionally regulates feeding. *Elife.* 2016;5.

33 Paxinos G, Franklin KB. *Paxinos and Franklin's the Mouse Brain in Stereotaxic Coordinates.* Academic press; 2019.

34 Hamelmann E, Schwarze J, Takeda K, et al. Noninvasive measurement of airway responsiveness in allergic mice using barometric plethysmography. *Am J Respir Crit Care Med.* 1997;156(3 Pt 1):766–775.

35 Nouraei SA, Giussani DA, Howard DJ, Sandhu GS, Ferguson C, Patel A. Physiological comparison of spontaneous and positive-pressure ventilation in laryngotracheal stenosis. *Br J Anaesth.* 2008;101(3):419–423.

36 Sheikhbahaei S, Gourine AV, Smith JC. Respiratory rhythm irregularity after carotid body denervation in rats. *Respir Physiol Neurobiol.* 2017;246:92–97.

37 Abbott SB, Coates MB, Stornetta RL, Guyenet PG. Optogenetic stimulation of C1 and retrotrapezoid nucleus neurons causes sleep state−dependent cardiorespiratory stimulation and arousal in rats. *Hypertension.* 2013;61(4):835–841.

38 Malheiros-Lima MR, Takakura AC, Moreira TS. Depletion of rostral ventrolateral medullary catecholaminergic neurons impairs the hypoxic ventilatory response in conscious rats. *Neuroscience.* 2017;351:1–14.

39 Xie X, Venit T, Drou N, Percipalle P. In mitochondria β-actin regulates mtDNA transcription and is required for mitochondrial quality control. *iScience.* 2018;3:226–237.

40 Shi Y, Stornetta RL, Stornetta DS, et al. Neuromedin B expression defines the mouse retrotrapezoid nucleus. *J Neurosci.* 2017;37 (48):11744–11757.

41 Malheiros-Lima MR, Totola LT, Lana MVG, Strauss BE, Takakura AC, Moreira TS. Breathing responses produced by optogenetic stimulation of adrenergic C1 neurons are dependent on the connection with preBotzinger complex in rats. *Pflugers Arch.* 2018;470 (11):1659–1672.

42 Díaz HS, Andrade DC, Toledo C, et al. Inhibition of brainstem endoplasmic reticulum stress rescues cardiorespiratory dysfunction in high output heart failure. 2021; 77(2): 718-28.

43 Guyenet PG, Stornetta RL, Bayliss DA. Central respiratory chemoreception. *J Comp Neurol.* 2010;518(19):3883–3906.

44 Eckert DJ, Malhotra A, Jordan AS. Mechanisms of apnea. *Prog Cardiovasc Dis.* 2009;51(4):313–323.

45 Burke PG, Kanbar R, Viar KE, Stornetta RL, Guyenet PG. Selective optogenetic stimulation of the retrotrapezoid nucleus in sleeping rats activates breathing without changing blood pressure or causing arousal or sighs. *J Appl Physiol.* 2015;118 (12):1491–1501. (1985).

46 Bach KB, Mitchell GS. Hypercapnia-induced long-term depression of respiratory activity requires alpha2-adrenergic receptors. *J Appl Physiol.* 1998;84(6):2099–2105. (1985).

47 Burgraff NJ, Neumueller SE, Buchholz KJ, Hodges MR, Pan L, Forster HV. Glutamate receptor plasticity in brainstem respiratory nuclei following chronic hypercapnia in goats. *Physiol Rep.* 2019;7 (8):e14035.

48 Sobrinho CR, Goncalves CM, Takakura AC, Mulkey DK, Moreira TS. Fluorocitrate-mediated depolarization of astrocytes in the retrotrapezoid nucleus stimulates breathing. *J Neurophysiol.* 2017;118 (3):1690–1697.

49 Suadicani SO, Brosnan CF, Scemes E. P2X7 receptors mediate ATP release and amplification of astrocytic intercellular Ca^{2+} signaling. *J Neurosci.* 2006;26(5):1378–1385.

50 Khan MT, Deussing J, Tang Y, Illes P. Astrocytic rather than neuronal P2X7 receptors modulate the function of the tri-synaptic network in the rodent hippocampus. *Brain Res Bull.* 2019;151:164–173.

51 Mulkey DK, Mistry AM, Guyenet PG, Bayliss DA. Purinergic P2 receptors modulate excitability but do not mediate pH sensitivity of RTN respiratory chemoreceptors. *J Neurosci.* 2006;26(27):7230–7233.

52 Plataki M, Sands SA, Malhotra A. Clinical consequences of altered chemoreflex control. *Respir Physiol Neurobiol.* 2013;189(2):354–363.

53 Guyenet PG, Bayliss DA. Neural control of breathing and CO_2 homeostasis. *Neuron.* 2015;87(5):946–961.

54 Dempsey JA, Smith CA. Pathophysiology of human ventilatory control. *Eur Respir J.* 2014;44(2):495–512.

55 Gourine AV, Llaudet E, Dale N, Spyer KM. ATP is a mediator of chemosensory transduction in the central nervous system. *Nature.* 2005;436(7047):108–111.

56 Guyenet PG, Bayliss DA, Stornetta RL, et al. Proton detection and breathing regulation by the retrotrapezoid nucleus. *J Physiol.* 2016;594(6):1529–1551.

57 Toledo C, Andrade DC, Lucero C, et al. Contribution of peripheral and central chemoreceptors to sympatho-excitation in heart failure. *J Physiol.* 2017;595(1):43–51.

58 Roger S, Pelegrin P, Surprenant A. Facilitation of P2X7 receptor currents and membrane blebbing via constitutive and dynamic calmodulin binding. *J Neurosci.* 2008;28(25):6393–6401.

59 Alves LA, de Melo Reis RA, de Souza CA, et al. The P2X7 receptor: shifting from a low- to a high-conductance channel - an enigmatic phenomenon? *Biochim Biophys Acta.* 2014;1838 (10):2578–2587.

60 Kopp R, Krautloher A, Ramirez-Fernandez A, Nicke A. P2X7 interactions and signaling - making head or tail of It. *Front Mol Neurosci.* 2019;12:183.